Available online at www.sciencedirect.com
SCIENCE DIRECT®
Earth and Planetary Science Letters 218 (2004) 317–330
EPSL
www.elsevier.com/locate/epsl

Oceanic oxygen-18 at the present day and LGM: equilibrium simulations with a coupled climate model of intermediate complexity

D. Roche [a,*], D. Paillard [a], A. Ganopolski [b], G. Hoffmann [a]

[a] *IPSL/Laboratoire des Sciences du Climat et de l'Environnement, CEA-CNRS, Bât. 709, Orme des Merisiers, 91191 Gif sur Yvette, France*

[b] *Potsdam Institute for Climate Impact Research, P.O. Box 60 12 03, 14412 Potsdam, Germany*

Received 21 July 2003; received in revised form 28 November 2003; accepted 3 December 2003

Abstract

An Earth system model of intermediate complexity, CLIMBER-2, is used to simulate the oxygen-18 content of the water masses ($H_2^{18}O$) in the oceans. Firstly, we forced CLIMBER-2 with the fluxes from the atmospheric general circulation model ECHAM. Simulated oceanic ^{18}O fields for the present day are in good agreement with data. Secondly, a water isotope module was developed to transport $\delta^{18}O$ in the atmosphere on a large scale and compute the ^{18}O fluxes to the ocean at the atmosphere–ocean interface using only variables already computed by CLIMBER-2. For the present day, we successfully represent oxygen-18 distribution in the Atlantic, Indian and Pacific oceans, and close agreement is also found when we compare modelled and observed $\delta^{18}O_w$:salinity relationships. During the Last Glacial Maximum (LGM), we find that the major differences in the ^{18}O oceanic fields (apart from the global oceanic enrichment due to ice-sheet build-up) are due to surface condition changes (surface temperature, shift in bottom water formation zones) and that no drastic changes occurred in the $\delta^{18}O_w$:salinity spatial relationship. In addition, we compute a calcite $\delta^{18}O_c$ field for the Atlantic and compare it to the available data to assess the variation between the LGM and the present day.

Keywords: O-18; paleoclimatology; modelling

1. Introduction

In this paper, we discuss the oxygen-18 stable isotope in two molecules: in water, as $H_2^{18}O$, and in calcite $CaC^{18}O^{16}O_2$. The ^{18}O in water can be measured in the three different phases that exist in the Earth system: in vapor (hereafter denoted $^{18}O_v$), in liquid as ocean water, runoff and rain (hereafter denoted $^{18}O_w$) and in ice (or snow). Huge amounts of data have been retrieved from various types of archives (foraminiferal calcite from sediment cores, ^{18}O in ice cores, pore-water measurements), each providing information about

* Corresponding author. Tel.: +33-1-69-08-88-62.
E-mail addresses: roche@lsce.saclay.cea.fr (D. Roche), paillar@lsce.saclay.cea.fr (D. Paillard), ganopolski@pik-potsdam.de (A. Ganopolski), hoffmann@lsce.saclay.cea.fr (G. Hoffmann).

0012-821X/04/$ – see front matter © 2004 Elsevier B.V. All rights reserved.
doi:10.1016/S0012-821X(03)00700-3

different aspects of the problem. In particular, the $\delta^{18}O_c$ [1] of foraminiferal calcite provides information about the local paleotemperature and $^{18}O_w$ (oxygen-18 composition of the surrounding water masses). One can use a paleotemperature equation to relate these different parameters, for example [1,2]:

$$T = 16.9 - 4.38(\delta^{18}O_c - \delta^{18}O_w) + 0.10(\delta^{18}O_c - \delta^{18}O_w)^2 \quad (1)$$

where the indices c and w stand for calcite and water respectively. One particular piece of information (T or $\delta^{18}O_w$) cannot be determined from these records: one has to fix one parameter to obtain the variation of the other. For example, it is often assumed that the benthic foraminifera signal during glacial times is mainly due to $\delta^{18}O_w$ variations, as the temperature of the bottom waters of the ocean cannot fall much lower than today, leading to an almost constant benthic temperature. Paleosalinities may be derived in a similar manner since it is often assumed that the $\delta^{18}O_w$:salinity relationship did not vary in the past climates allowing local salinity to be found from a measured $\delta^{18}O_w$. More recently, porewater measurements in sediment cores [3,4] have provided a more direct constraint on the estimation of the paleo-$\delta^{18}O$ of seawaters. These measurements are sparse, but will be used to validate our results.

In order to assess whether these assumptions are justified or not, a modelling approach is clearly needed. Some modelling of the ^{18}O has already been done using oceanic general circulation models (OGCMs) [5–7]. However, no studies have been done in coupled atmosphere–ocean models. OGCMs generally use the CLIMAP sea-surface temperature reconstruction [8] as a boundary condition for Last Glacial Maximum (LGM) conditions, and fix the water fluxes at the oceanic surface. This leads to inconsistent fields between temperature, ^{18}O, water fluxes, and salinity. The resulting relationships from such studies may be potentially biased by this inconsistency. Moreover, the use of a fixed temperature at the ocean surface as a boundary condition may have a non-negligible effect on the modelling of ^{18}O in calcite.

In the following, we conduct a study in two parts. First, we included ^{18}O as a passive tracer in the oceanic component of the CLIMBER-2 model, using the fluxes from the atmospheric general circulation model (AGCM) ECHAM [9,10] at the ocean–atmosphere interface as a forcing. The results obtained allow us to validate the ocean transport module for $^{18}O_w$. In a second step, a parametrization of the ^{18}O flux at the ocean–atmosphere interface is developed which uses the water fluxes computed in CLIMBER-2. This allows us to simulate ^{18}O for different climates.

2. CLIMBER-2

We use the Earth system model of intermediate complexity CLIMBER-2, a coarse-resolution fully coupled model designed for long-term simulations. It is composed of a 2.5-dimensional statistical-dynamical atmosphere, with spatial resolution of $10° \times (360°/7 \approx 51.4°)$. The ocean model is composed of three zonally averaged basins (Atlantic, Indian, Pacific) resolved on a 2.5° latitudinal grid, with 20 uneven vertical layers. It is based on the zonally averaged equations from [11]. The Arctic and Antarctic oceans are parts of these three oceanic basins. In this work, we do not use an interactive ice-sheet model, instead ice sheets are prescribed in accordance with paleoclimate reconstructions. The model is able to capture the main features of the modern climate [12] as well as those of the LGM [13] and compares favorably with paleoclimatic simulations with general circulation models [14]. It also successfully simulates rapid climatic changes during glacial times [15]. Because this model includes all major components of the climate system (atmosphere, ocean, biosphere, cryosphere) and has a fast turnaround time, it is convenient to explore past climates. As the $^{18}O_w$ is conserved in the ocean, we only need to advect and diffuse it in the ocean

[1] In paleoclimatology, the isotope composition is expressed as its deviation to the V-SMOW common standard (isotope ratio of $R^{18}_{Std} = 2005.2 \times 10^{-6}$) as: $\delta^{18}O = ((R_{18}/R^{18}_{Std}) - 1) \times 1000$ expressed in ‰.

module of CLIMBER-2. We then apply the fluxes at the ocean–atmosphere interface. In the following, two methods are used for this: (a) using the ^{18}O simulated by the AGCM ECHAM (the CLIM-E version hereafter) and (b) parametrizing the fluxes within the CLIMBER-2 model (the CLIM-P version hereafter).

3. ECHAM and the CLIM-E version

The AGCM ECHAM directly represents the stable isotopes in the atmosphere. We used here the present-day equilibrium fluxes produced by this model to force CLIMBER-2, that is water fluxes (evaporation and precipitation) and the isotopic content ($\delta^{18}O$) of these fluxes [10]. With these fluxes we compute an equilibrium field for ^{18}O in the ocean of CLIMBER-2. We use this method only as a first step to validate the transport of the water tracer in our coupled model. We are nonetheless facing a consistency problem, as noted in Section 1. While the water fluxes of ECHAM and CLIMBER-2 are similar, both in values and in spatial variations, they are not strictly identical. This means that a computed $^{18}O_w$ with the water fluxes of ECHAM is not consistent with the salinity computed directly with CLIMBER-2. To compare to observations, a usual method is to compare $\delta^{18}O_w$:salinity relationships. For consistency reasons, we here compute a second salinity (hereafter called 'artificial salinity') with the water fluxes from ECHAM. This artificial salinity will not be identical to that simulated by CLIMBER-2, and will only be used as an additional passive tracer. That is, the artificial salinity has no effect on the ocean dynamics and convection. The discrepancies between the two salinities will help us to understand the differences between the water fluxes of ECHAM and CLIMBER-2.

This method does not ensure the global conservation of the $H_2^{18}O$ content of the ocean. The $H_2^{18}O$ is conserved in ECHAM, but we only use the fluxes over the oceans. Consequently the runoff is taken from CLIMBER-2 and the $H_2^{18}O$ is not necessarily conserved in CLIM-E. To avoid any drift in the overall content of the oceans, we integrate all fluxes to the ocean and subtract uniformly the difference to global equilibrium. This CLIM-E version is only used for the present-day equilibrium simulation. All other experiments are performed with the CLIM-P version.

4. Present-day equilibrium with CLIM-E

We first analyze the results obtained by forcing the $^{18}O_w$ in CLIMBER-2 with fluxes from the ECHAM model. The CLIMBER-2 model itself is equilibrated (10 000 year run) under present-day (pre-industrial) boundary conditions [12].

4.1. Model–data comparison for $\delta^{18}O_w$

In Fig. 1, the surface $\delta^{18}O$ obtained using CLIM-E is compared to data (left column). The reference data for $\delta^{18}O_w$ are the GISS oxygen-18 database [6,16,17], aggregated over the CLIMBER-2 grid to allow easy comparison. Note that the Mediterranean points of the GISS database are plotted together with the Indian Ocean sector, as is done in CLIMBER-2, to allow a direct comparison. At first glance, and given the resolution of our model, we obtain good agreement between the two fields. Latitudinal variation is correctly captured overall, giving low values at high latitudes, a maximum in the tropics and a small relative minimum at the equator. However, discrepancies in the details are visible. The two main ones are the underestimated maximum in the northern tropical belt of the Indian Ocean and the too low and homogeneous minimum of the Nordic Seas and Arctic Ocean. As the ocean module of CLIMBER-2 is based on a multibasin zonally averaged model, it is not possible to simulate zonal variations in one particular ocean. For the northernmost part of the Arctic in the Atlantic sector of the model, we failed to reproduce the observed values that are in the range -1.5 to -2.0‰. Instead, we obtained much lower values, below -3‰. One can also observe that our modelled tropical maximum in the Atlantic is slightly too low. This is due to an evaporation–precipitation balance that is not positive enough in those

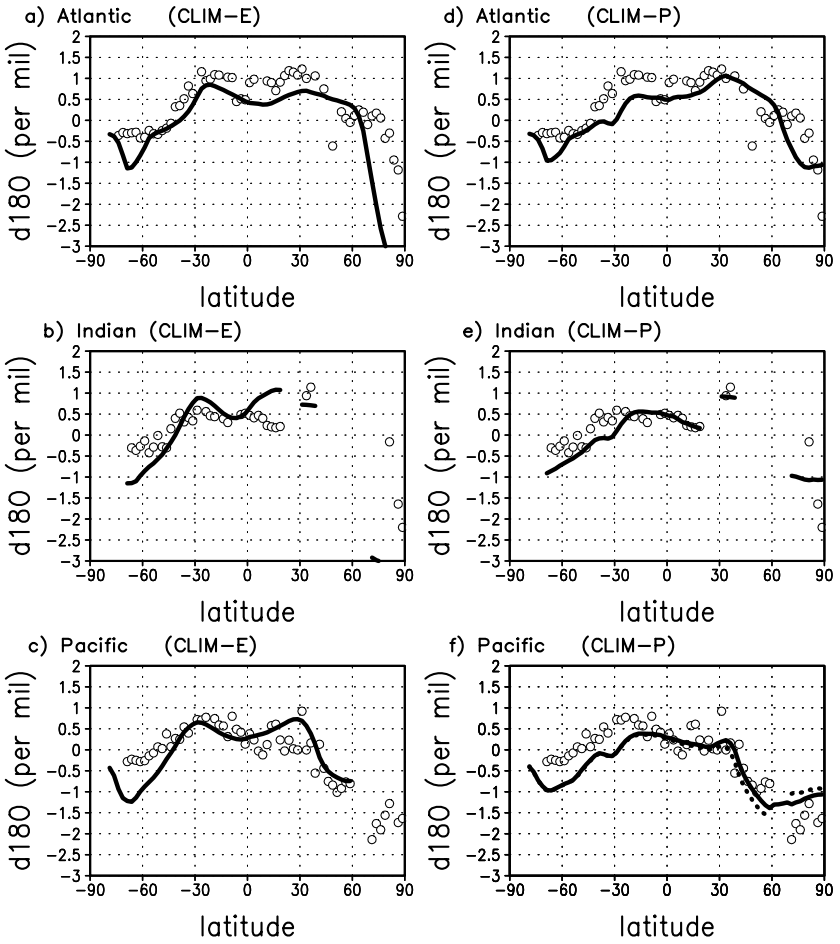

Fig. 1. Comparison of modelled and observed $\delta^{18}O_w$ surface values in the world ocean. Open circles are data points [6,16,17] aggregated on the CLIMBER-2 oceanic grid whereas the solid line shows modelled values. The left column presents the results for the CLIM-E version, the right column for the CLIM-P version. In panel f, the dotted line shows the result for the CLIM-P version with a closed Bering Strait, the solid line showing the version with an opened Bering Strait (see text for discussion).

regions when we use the fluxes of ECHAM aggregated on the CLIMBER-2 ocean grid. Despite these shortcomings, the general qualitative agreement is encouraging.

4.2. Salinity to artificial salinity comparison

Before comparing the $\delta^{18}O_w$:salinity relationship from our model to the data, we have to verify that the salinity and artificial salinity values are closely related. As shown in Fig. 2, we have a good linear relationship between the two salinities, except for a few points with high artificial salinities. The regression computed between the two salinities exhibits a slope larger than 1 (which should be obtained if they were identical). This is due to the freshwater fluxes of ECHAM which induce slightly larger salinity gradients than the CLIMBER ones, hence the slope larger than 1.

A comparison between the evaporation minus precipitation water fluxes in these latitudinal bands from CLIMBER-2 and ECHAM (not shown) confirms this.

4.3. Oxygen-18:salinity relationship

We now compare the $\delta^{18}O_w$:salinity relationship obtained from our model (that is, with arti-

ficial salinity) to the data. Here, salinity refers to the artificial salinity computed with the water fluxes of ECHAM. Salinity and $\delta^{18}O_w$ fields in the oceans differ only from the fluxes at the ocean–atmosphere interface since salinity reflects only freshwater fluxes, whereas $\delta^{18}O_w$ reflects both freshwater fluxes and their isotopic content. One approach is to plot the $\delta^{18}O_w$:salinity relationship for the surface (or global) oceans, as has been done in Fig. 3. Fig. 3a shows the data while Fig. 3b presents the model results, including regression lines. Two regression lines are given for the model results: a main one for most points, and the second one for the low-latitude points. The regression line for the data (in the salinity range 32–37‰) shows a slope of ~0.59, while the model exhibits a slope of ~0.60. The equatorial-tropical surface points, in the model, display a slope of 0.18 whereas no such line can be drawn for the data, when averaged on the CLIMBER-2 grid. However, such values may be found when drawing regional regression lines with the raw (unaveraged) data. It is interesting to note that the Mediterranean waters (few points at 37‰ in salinity) fall on the equatorial-tropical secondary line. The overall modelled results are thus in quite good agreement with the data.

As shown above, we successfully represent the $\delta^{18}O_w$ in the ocean for the present day with the CLIM-E version. The use of this version is, however, limited for two reasons. First, even if the discrepancy between the two salinities due to the water fluxes to the oceans is not strong when computing equilibria for the present day, this may not be the case when simulating other climates. Second, this approach limits the application of our model to periods already assessed using ECHAM. There is therefore a need for a version of CLIMBER-2 that can compute all of the required fields by itself. This is done in the following section with the CLIM-P version.

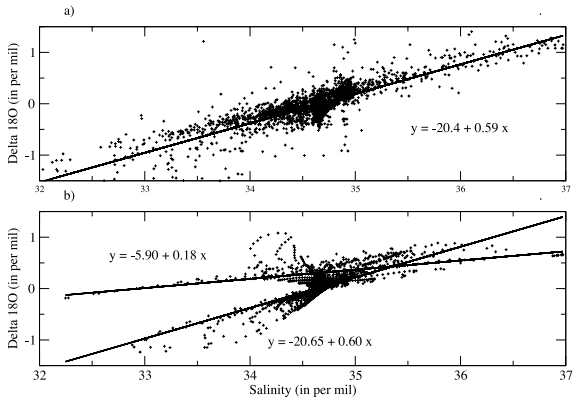

Fig. 3. $\delta^{18}O_w$:salinity relationship for the world ocean. (a) Observations aggregated on the CLIMBER-2 grid [6,16,17], correlation coefficient for the regression line is 0.59. (b) Modelled results using CLIM-E. In panel b, the line with a slope of 0.18 is for the tropics, the other line for all points but without the tropics, with correlation coefficient 0.65.

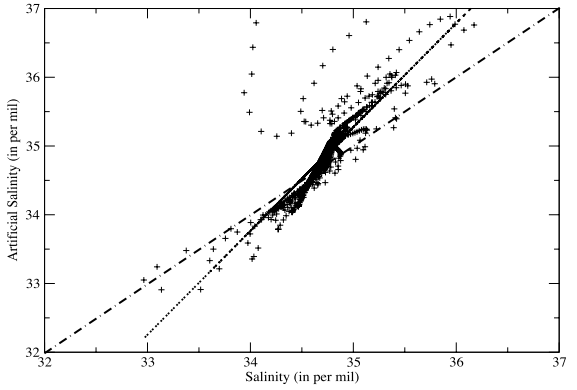

Fig. 2. Artificial salinity to salinity for the CLIM-E version. Surface points from the Atlantic basin of CLIMBER-2. The dotted line gives the linear regression of this plot. The dash-dotted line is the 1:1 line.

5. The oxygen-18 module: the CLIM-P version

The CLIM-P version is based on a module that computes isotopic fluxes using simple parametrizations at the atmosphere–ocean interface. The isotopic flux to the ocean may be expressed as:

$$F^{18}_{A\rightarrow O} = F_P(R^{18}_P - R^{18}_0) + F_E(R^{18}_E - R^{18}_0) + F_R(R^{18}_R - R^{18}_0) \quad (2)$$

where F_is are the water fluxes into the ocean and $R_i{}^{18}$s are the isotopic contents of these fluxes. The indices P, E, R and O represent precipitation, evaporation, runoff and ocean-surface waters, respectively. Water fluxes into the ocean are already computed in CLIMBER-2. To parametrize their

isotopic content, we used a formula similar to [18] for precipitation and the formula of [19] for evaporation, expressed as:

$$\delta_P^{18} = 0.345T - 0.0022P + C_i \quad (3)$$

$$\delta_E^{18} + 1 = \frac{1-k}{1-h}\left[\frac{1}{\alpha}(\delta_{O_c}^{18} + 1) - (\delta_{Vap}^{18} + 1) \times h\right] \quad (4)$$

where T and P are surface air temperature and precipitation, $\delta_{O_c}^{18}$ and δ_{Vap}^{18} are the $\delta^{18}O$ of the surface ocean and water vapor, k is a dimensionless constant ($k = 6 \times 10^{-3}$), h is the relative surface humidity over the ocean and C_i represents a large-scale transport correction term, explained hereafter. Although the formula of [18] was initially developed for continental precipitations, we checked that the slope with respect to T and P is also correct for marine precipitations by comparing with the measurements of the GNIP database (International Atomic Energy Agency-Global Network of Isotopes in Precipitation). The isotopic content of water vapor is taken to be in equilibrium with the liquid phase written as:

$$R_{Vap}^{18} = \frac{1}{\alpha} R_P^{18} \rightarrow \delta_{Vap}^{18} = \frac{1}{\alpha}\delta_P^{18} + \left(\frac{1}{\alpha} - 1\right) \quad (5)$$

where α is the liquid/vapor fractionation coefficient defined as [20]:

$$\ln(\alpha) = \frac{1.137 \times 10^3}{T^2} - \frac{0.4156}{T} - 2.0667 \times 10^{-3} \quad (6)$$

where T is in Kelvin. Surface air temperature, precipitations and relative humidity are computed by CLIMBER-2.

The resulting isotopic fluxes are applied to the upper layer of the model and the $\delta^{18}O_w$ is advected and diffused in the ocean. To conserve $^{18}O_w$, based on physical processes, one must consider the atmospheric hydrological cycle. We will compute the C_i terms by defining a nine-box isotopic balance model of the atmosphere. Therefore, these boxes are chosen in order to minimize meridional transport between them. As can be seen from fig. 3, page 4 in [12], the annual mass transport in the atmosphere, zonally averaged over the globe, shows an advective pattern in cells. From this, three different regions may be defined: the Hadley cell region (from −30 to 30°N over an annual mean), and two outer Hadley regions, one northern and one southern. In each of these regions, water is essentially conserved. That is, what evaporates within the tropical region re-precipitates there. As our region boundary is defined by the divergence of the latitudinal advective mass transport, there is no latitudinal advective transport from one region to another. Hence, there is no water transport due to advection at these boundaries. Since the tracer we are attempting to model is $H_2^{18}O$, if water is conserved, then $H_2^{18}O$ must also be conserved in each region. Because our aim is to model $\delta^{18}O_w$ for each ocean basin, we need such a description over an ocean-basin spatial scale. However, as there is some large-scale zonal interbasin transport (for example above the Panama regions between the Atlantic and Pacific oceans), the same regions defined over such a scale do not conserve water. As water vapor transport is explicitly computed in the atmosphere module of CLIMBER-2 [12], we are able to derive these interbasin fluxes from water conservation. We then compute a $\delta^{18}O_w$ content for these fluxes to close the isotopic balance for each box (Fig. 4). The fluxes between two cells of the same basin (for example F_{23} and F_{21} in the Atlantic) represent the diffusion at the

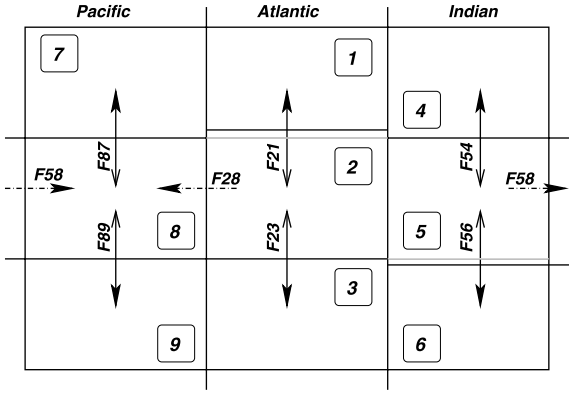

Fig. 4. Nine-box model for the mass balance of the isotopic budget over the oceans defined by the three ocean basins of CLIMBER-2 and the seasonally varying location of the Hadley cells. The dash-dotted arrows show the global-averaged direction of interbasin transport, and double arrows indicate diffusion at the border of the cells. No fluxes are assumed between the Atlantic and Indian basins. Adding a strong flux between the southern (9,3,6) cells would not change the obtained results. See text for more details on the definitions of the boxes.

border of each cell. These fluxes are much smaller than the net flux ($E-P$), or than typical advective transports. The zonal isotopic fluxes are expressed as:

$$F_{ij}^{18} = F_{ij}\frac{h_i}{h_j}(\delta_v^{18}(i)-\delta_v^{18}(j)) \quad (7)$$

where F_{ij} is the water flux, h_i the specific humidity of box i, and $\delta_v^{18}(i)$ the ^{18}O content of the vapor. The limits of these boxes vary over time with the seasonal fluctuations of the Hadley cell and are dynamically computed in each basin separately. The correction term C_i appears in the R_i^{18} terms, as follows:

$$R_P^{18} = (\delta_P^{18}\times 10^{-3}+1)R_{Std} = ((0.345T-0.0022P+C_i)+1)R_{Std} \quad (8)$$

In each box i, we write the conservation of isotopes as follows:

$$\int_S -F_P(R_P^i-R_0)+F_E(R_E^i-R_0)-F_R(F_R^i-R_0)+ F_{ij}(R_{Vap}^i-R_{Vap}^j)+F_{ki}(R_{Vap}^k-R_{Vap}^i)dS = 0 \quad (9)$$

where notations are the same as for Eq. 2. The unknown C_is are computed by solving a nine-linear-equation system provided by Eqs. 9 and 8 for each box. For example, in the present-day simulations, this parameter C_i has a value around $-12.38‰$ in the tropics, to be compared to Farquhar's constant of $-11.88‰$. It should be noted that this correction term is based on sound phys-

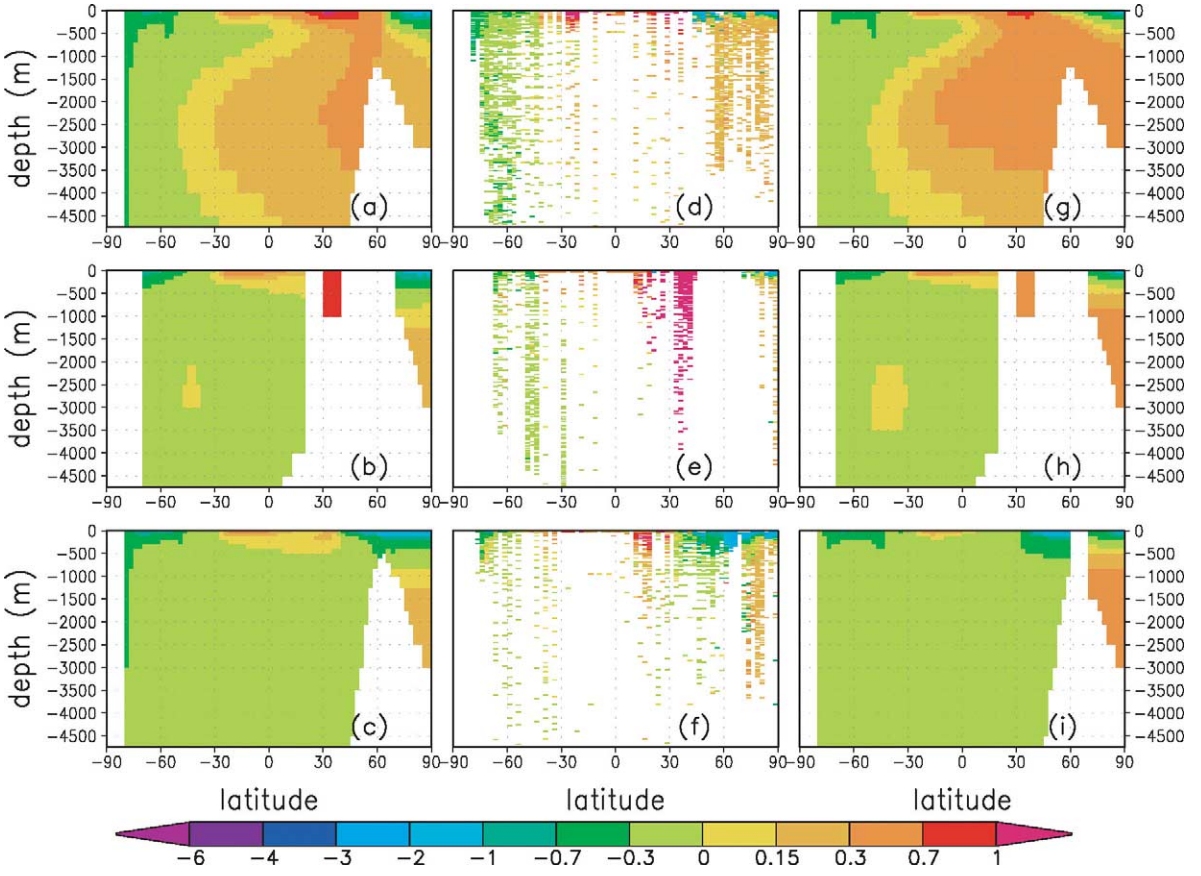

Fig. 5. Latitude–depth section for the $^{18}O_w$ fields in the world ocean. The left column shows results from the model in the CLIM-P version for the present day, the middle column presents the data [6,16,17], and the right column shows the model results in the CLIM-P version for the LGM. Panels a, d and g show Atlantic Ocean sections, b, e and h show Indian Ocean sections and c, f and i show Pacific Ocean sections. All are given with the same color scale, shown by the color bar, labelled in ‰.

ical assumptions, and depends on the climate. It is computed dynamically by the model for any climate we would like to simulate. Runoff in CLIMBER-2 is a function of relative soil moisture and precipitation [12] and is added to the ocean as a freshwater flux. For the isotopic content, we assign to the runoff the same $\delta^{18}O_w$ value as local precipitation. Calving is assumed to have a prescribed $\delta^{18}O$ content of $-30‰$ [7]. Isotopic changes due to sea ice are not considered in this version of the model. However, because there is no large accumulation of sea ice, there are no ^{18}O mass balance problems.

The resulting water isotope module allows us to compute the oxygen-18 fields in the ocean without any kind of external forcing or restoring conditions, and hence to simulate these fields under various climatic conditions since it is based only upon physical considerations. In the following, we explore two 'classical' climate equilibria: present day (pre-industrial) and LGM.

6. Present-day equilibrium with CLIM-P

The model was integrated to equilibrium, under present-day conditions as in [12], that is present-day solar forcing (insolation), pre-industrial CO_2 atmospheric concentration (280 ppm) and prescribed present-day ice sheets.

6.1. Model–data comparison in $^{18}O_w$

Surface $\delta^{18}O_w$ values for present-day conditions in CLIMBER-2 are compared to data [6,16,17] in Fig. 1 and latitude–depth sections are in Fig. 5.

Looking first at the surface distributions, one can see that we reproduce well both the latitudinal gradients and the absolute values at most points. We found a relative minimum at the equator between the two tropical maxima, for the Atlantic and the Pacific oceans. This feature also exists in the data, but with some slightly higher values than in our model, in particular for the south tropical maximum. Simulated $\delta^{18}O_w$ values in the Atlantic are altogether higher than in the Pacific and Indian oceans, which is a crucial feature of the data, indicating we capture correctly the interbasin ^{18}O transport. For the Arctic Ocean however, our simulated values are too heavy in the Pacific sector, but mainly correct in the Atlantic and Indian sectors, although there is some scatter in the data. Our Arctic Ocean results are very similar in each sector, since the three basins are connected in this region. As we do not consider the Bering Strait, which is closed in the standard version of CLIMBER-2, there is a step in $\delta^{18}O_w$ values around 60°N in the Pacific. This is unrealistic, and may have a strong influence on the surface $\delta^{18}O_w$ content of all oceans north of 60°N [21]. We will investigate this point further. Our results for the surface $\delta^{18}O_w$ are nonetheless quite good, given the simple parametrization used here.

At depth (Fig. 5), we again obtain a fairly good $\delta^{18}O_w$ distribution in the Atlantic, Indian and Pacific oceans (apart from the Arctic regions). In the Atlantic, we find a very close agreement as far as one can infer from the limited number of measurements. The surface minimum at high southern latitude is correctly represented in all sectors. However, more regional details are missing from our results; the limited (in space) minimum area around 60°S at depth in the Indian Ocean is not reproduced and we obtain some slightly too low values in the Indian Ocean around 500 m depth at 10°N. This probably comes from the difficulty of representing a precise circulation in the Indian Ocean with a zonally averaged model, since the real circulation is essentially zonal in this part of the world oceans.

6.2. Influence of the Bering Strait

As noted before, the absence of the Bering Strait in the model would affect the $\delta^{18}O_w$ field in the Arctic. We therefore performed a run with an opened Bering Strait, that is with a connection between the Arctic and north Pacific oceans. In order to have a connection with a few cells' depth, we opened a strait 500 m deep, although the real value is less than 100 m. As shown in Fig. 1f, the existence of the Bering Strait has little effect on the $\delta^{18}O_w$ field in the north Pacific sector, although surface $\delta^{18}O_w$ is lower in the Arctic north of 60°N, and higher values are seen at

30°N (due to slightly reduced surface currents). These changes result in a better fit to the data, even though differences are very small (maximum changes are around 0.2‰), contrary to what was found by [21]. In the other basins, no changes at all could be seen.

In the following, we will use this version with the opened Bering Strait when referring to 'present day' since these results are slightly better than those shown earlier (see Fig. 5).

6.3. Oxygen-18:salinity relationship

In Fig. 6, we show the simulated $\delta^{18}O_w$:salinity relationship for the world oceans. Two regression lines are drawn: a global one for almost all points, with a slope of 0.56, and a local one for the north Pacific and Arctic oceans, with a slope of 0.31. As we have not successfully represented the Arctic $\delta^{18}O_w$, the second regression line does not correspond to any clear trend in the data. However, one still sees that, when compared to the raw data (without averaging on the CLIMBER-2 grid, see inset in Fig. 6), these north Pacific and Arctic points still fall within the data range. The inability to obtain the correct values for the Arctic points may show that we have neglected a crucial process there (e.g. sea ice?) or that our simple assumptions are not always sufficient to explain the $\delta^{18}O_w$ fields on a regional scale. Despite this, we have a fairly good agreement with the data whose global regression line has a slope of 0.59, close to our simulated value, 0.56. To compare in even more detail our results to the data, we computed regression lines for $\delta^{18}O_w$:salinity relationships for surface points in three different regions (taken over all basins): low latitudes (30°S to 30°N), mid latitudes (30–

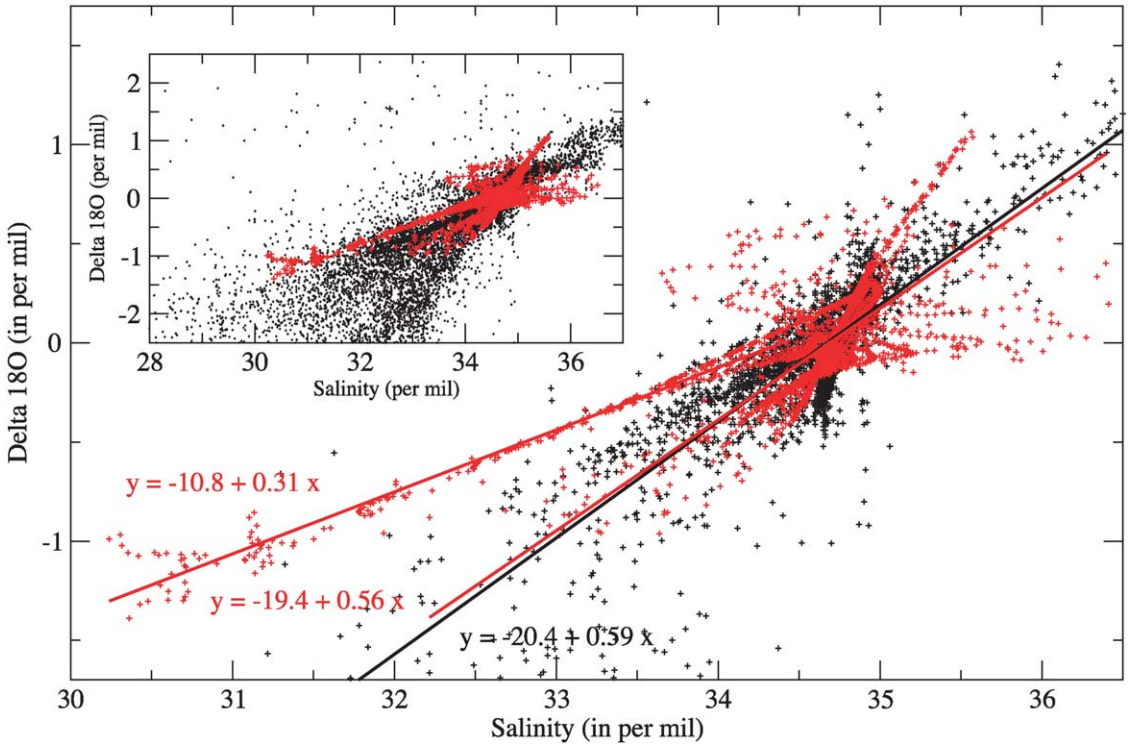

Fig. 6. $\delta^{18}O_w$:salinity relationship for the world ocean with all points at all depths using CLIM-P. Red points are from the model, black points are from data (averaged on the CLIMBER-2 grid). Red lines shows the regression lines for the red points (the one with slope 0.31 for the arctic points with correlation coefficient 0.98, the one with slope 0.56 for the others with correlation coefficient 0.59). Inset: same color definitions, but with raw (unaveraged) data [6,16,17].

60°N,S) and high latitudes (more than 60°N,S). Obtained results for the model (resp. data) are: low-latitude slope = 0.06 (data 0.34) with $R^2 = 0.16$ (data 0.7); mid-latitude [two lines] slope = 0.36 [S] and 1.17 [N] (data 0.47) with $R^2 = 0.97$ and 0.99 (data 0.97); high-latitude slope = 0.28 (data 0.2) with $R^2 = 0.93$ (data 0.7). This shows that apart for the low latitudes where our model points are scattered without much linear relationship, modelled regional regression lines are quite consistent with the data. All these results are therefore encouraging. In the following, we explore the same type of results for the LGM.

7. LGM equilibrium

We now run the model using a typical glacial forcing [13]: insolation for 21 000 years BP, CO_2 atmospheric concentration down to 200 ppm, prescribed ice sheets and lower sea level using reconstructions from the ICE-3G model [22]. During glacial times, the build-up of huge ice sheets, with a $\delta^{18}O$ content between −30‰ and −35‰, enriched the oceans in this isotope. Globally, oceans were 1.05 ± 0.2‰ higher in $\delta^{18}O_w$ [23], depending upon the reconstruction used. As we do not have an interactive ice-sheet model that accommodates such changes in ^{18}O connected to our model, this effect is not taken into account: since simply adding this 1.05‰ change would be of little use, we maintain the overall content identical to the present day. Therefore, the only changes that are likely to affect the $\delta^{18}O_w$ distribution are changes in the hydrological cycle, and ocean circulation.

7.1. LGM to present-day $^{18}O_w$

Results for an equilibrated LGM run are shown in Fig. 5 and compared to present-day modelled results. One can see some differences for the Indian and Pacific oceans. In both basins, intermediate-depth isotopic contents around 60°S are slightly depleted in $\delta^{18}O_w$, due to some small changes in the circulation around the Antarctic. In the Pacific, surface waters are somewhat depleted around 40°N during the LGM relative to the present day, due to small changes in the freshwater budget in the tropical-equatorial regions (mainly reduced evaporation due to the cooler temperature).

Changes are more significant in the Atlantic. The isotopic content of the surface waters is depleted and the north tropical maximum is shifted southward. This is due, again, to changes of surface conditions at the LGM in these regions. The North Atlantic down to 3000 m depth shows an enhanced isotopic content. This is due to the southward shift of the region of deep water formation, towards a region with higher isotopic content. Altogether, the glacial North Atlantic waters have an enhanced isotopic content of ∼0.1‰ at the LGM.

At the bottom of the basin, where Antarctic bottom water (AABW) dominates, the ^{18}O isotopic content is slightly reduced. This is the result of enhanced Antarctic bottom formation, which still has a very low content during the LGM. This variation is, however, very small, from ∼−0.1‰ in the south to around 0.0‰ in the north. A constraint to validate these changes is provided by pore-water measurements [3,4]. According to such measurements, the deep Atlantic waters would have changed by 0.8 ± 0.1‰ in the north and up to 1.3 ± 0.1‰ in the south (see Fig. 8a, where these data points are indicated on the CLIMBER-2 $\delta^{18}O_w$ fields). Taking into account the global effect of ice volume (1.05 ± 0.2‰) in our results leads to meridional gradients one order of magnitude smaller than what is observed in the data (between 1.02 and 1.08‰ compared to 0.7–1.3‰). More precisely, one can see from Fig. 8a that we get qualitatively the same latitudinal gradient in the deep Atlantic. We do have lower values in the north and higher values in the south, as presented in [4], while our results show much too small variations in $\delta^{18}O_w$ for the deep Atlantic, indicating that our model sensitivity to the changes in the deep Atlantic for LGM times is too low. In particular, we may not reproduce correctly the predominance of $\delta^{18}O_w$-depleted AABW in the deep North Atlantic. To obtain a better agreement with the data [3,4], we would need a strongly enhanced AABW in the deep At-

lantic, whereas our simulation only shows a slightly enhanced one (by 3 Sv). This comparison is interesting, as it is independent of any other estimations.

7.2. Oxygen-18:salinity relationship

In Fig. 7, where both LGM and present-day $\delta^{18}O_w$:salinity relationships are shown, one can immediately see that there are only a few changes in the repartition of the points, and minor changes in the inferred slopes. This is not surprising, as we have only small changes in both the $\delta^{18}O_w$ and salinity fields. Regionally, the Arctic points are shifted toward a lower $\delta^{18}O_w$ content (mainly due to enhanced calving at the LGM), therefore modifying the regression slope for these points. The LGM slope is 0.35, where the present-day one is 0.31. For the other points, some differences also exist for the high southern latitudes, which lead to a slope of 0.61 for the LGM instead of 0.59 for the present day. All together, the changes in the regression lines are relatively small and are mainly related to the high latitudes. Given the resolution of the model and the assumption made when simulating the $^{18}O_w$ fields, we may say that there is almost no change in the spatial slope of the $\delta^{18}O_w$:salinity relationship between the LGM and the present day. Remember, however, that paleosalinity reconstructions are based on the assumption that the $\delta^{18}O_w$:salinity relationship derived from modern data (spatial relationship) is valid through time (temporal relationship) [24,6]. The stability of the global spatial slope shown here does not ensure stability of local $\delta^{18}O_w$:salinity relationships through time.

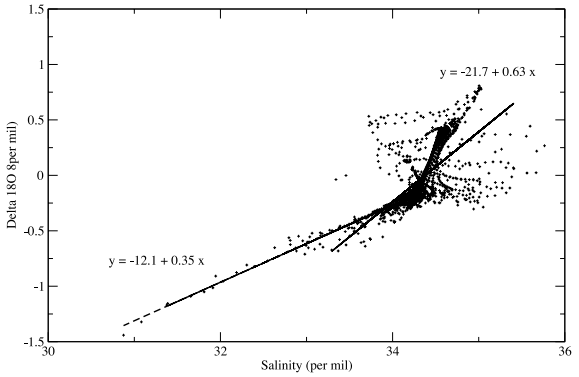

Fig. 7. Modelled $\delta^{18}O_w$:salinity relationship for the LGM as found from CLIM-P. Two lines are given: one for the Arctic points (with slope 0.35), another one for all points but the Arctic (with slope 0.63). All points in all basins and depths are used.

8. Calcite in the Atlantic at LGM: a modelling attempt

Since the CLIMBER-2 model provides us with simulated $^{18}O_w$ and temperature distributions, we may use Eq. 1 in a reversed form[2] (that is with δ_c as a function of $^{18}O_w$ and temperature) to compute the δ_c in the oceans. In the following, we will refer to the isotopic measurements in foraminiferal calcite as $\delta^{18}O_c$ whereas simulated calcite in equilibrium with $\delta^{18}O_w$ will be referred to as δ_c. This is shown in Fig. 8b, for the Atlantic, and compared to data [25–32] from sediment cores (Fig. 8d). Both are plotted as LGM–present-day differences. In this figure, we added the overall $\delta^{18}O_w$ difference due to ice-sheet build-up to our simulated fields (that is, 1.05 ± 0.2‰, as noted before), in order to allow direct comparison between data and modelled results.

From the data, differences between LGM and modern values are higher in the deep North Atlantic ($\Delta^{18}O \approx 1.9$‰)[3] than in the deep South Atlantic ($\Delta^{18}O \approx 1.7$‰). From our model, one immediately sees that most of the deep North Atlantic is around $\Delta^{18}O \approx 1.24$‰, whereas the deep South Atlantic is around $\Delta^{18}O \approx 1.3$‰, except for the southernmost part which reaches 1.36‰, meaning that the modelled signal is globally too small, and varies latitudinally in opposition to the data. As discussed before, we have already slightly too small $\delta^{18}O_w$ modifications when compared to data (by around 0.2‰), but with the correct latitudinal gradient. As the relationship between δ_c, $\delta^{18}O_w$ and temperature is linear, the temperature gradient has to be incor-

[2] From Eq. 1 we obtain: $\delta_c = 21.9 + \delta^{18}O_w - \sqrt{310.61 + 10T}$.

[3] $\Delta^{18}O = \delta^{18}O(\text{LGM}) - \delta^{18}O(\text{present day})$.

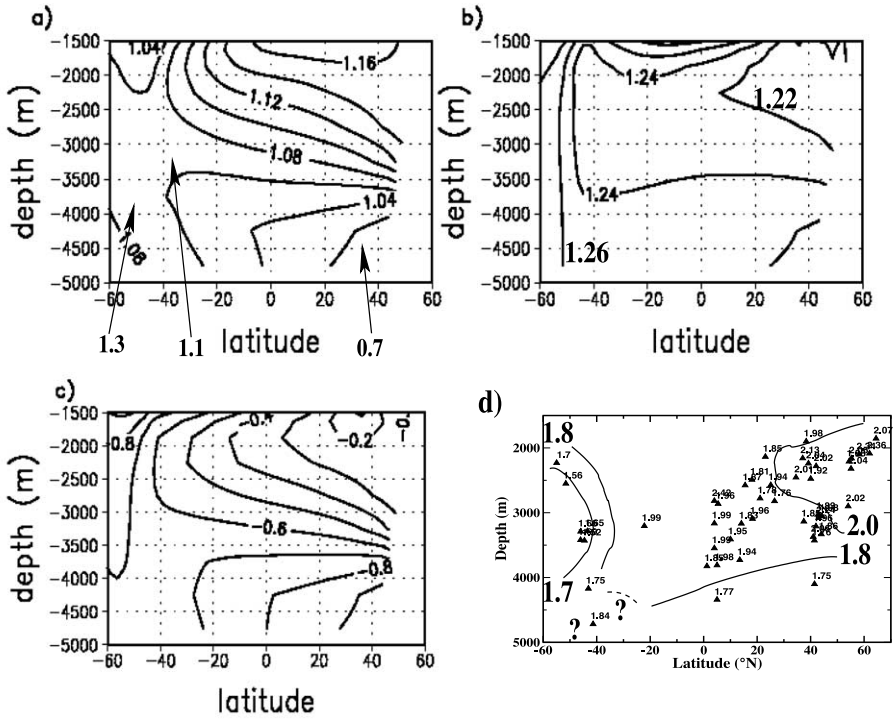

Fig. 8. Latitude–depth differences (LGM–modern) for the Atlantic Ocean. Panels a–c give the model results, panel d shows data [25–32]. Panel a gives $\Delta^{18}O_w$ (labelled in ‰), b gives $\Delta^{18}O_c$ (labelled in ‰), c gives ΔT (labelled in °C), d gives $\Delta^{18}O_c$ in data (labelled in ‰). Labelled arrows in panel a show data points from [4], also given in ‰. To allow for an easy comparison between model and data, 1.05‰ is added to panels a and b to account for the glacial ice-sheet build-up.

rect in the model. Today, the area of AABW formation in the southern ocean is very cold, and could not cool much more during glacial times, due to the limitation of the freezing point. There is potential, however, to reduce significantly the temperatures in the North Atlantic. In our model, we indeed reduce the very southern ocean by only −0.7°C, while in the rest of the Atlantic basin, the cooling increases northward, from −0.7°C at 20°S, to −0.9°C at 60°N (Fig. 8c). As we have globally too low variations in $^{18}O_c$ between the present day and glacial times, this means that our deep ocean is not cold enough during the LGM. For the latitudinal variations, it appears that our North Atlantic at depth does not cool enough relative to the southern Atlantic. It should be much colder, with an additional −1°C for the southern part and ∼−3°C for the northern part, in order to account for the calcite changes. Such temperature changes are indeed estimated from pore-water data [4] and may be due to the AABW formation that is not strong enough at the LGM in the model, as noted before. Evaluating δ_c with such temperature changes would be in better agreement with data. They are, however, not found in our model. Enhancing the overturning in the AABW branch would bring colder waters in the bottom of the Atlantic and there are indications [33–35] that this may have been the case during the LGM.

This comparison to data is instructive, since it suggests possible improvements of the model.

9. Conclusions

In this work, we studied the oceanic ^{18}O content under two different climate conditions. We first forced the ocean of our coupled model, CLIMBER-2, with the freshwater fluxes from an

AGCM, ECHAM, and computed a present-day equilibrium. The results obtained show good agreement with available data, both for $\delta^{18}O_w$ and for the $\delta^{18}O_w$:salinity relationship. We then developed an isotopic module to compute directly the $\delta^{18}O_w$ in the ocean part. This was done for the first time in a coupled ocean–atmosphere model, without any water flux prescription or fixed sea-surface temperatures. This is a important prerequisite to study past climate for a wide range of periods with good confidence. Although the isotope module is based on rather simple equations, we obtain some fairly good results when simulating present-day fields for $\delta^{18}O_w$ and the for $\delta^{18}O_w$:salinity relationship. The results are not entirely satisfying for the Arctic Ocean where the coarse resolution of the model is a strong limitation. The same study made for the LGM revealed that: (1) the $\delta^{18}O_w$ distribution is not very different at that time, apart from the Atlantic which shows an enhanced isotopic content at depth, resulting from changes in the area of deep water formation, and (2) the gradient of the global regression line in the $\delta^{18}O_w$:salinity relationship does not differ very much from the present-day one. Finally, the comparison of the computed $\delta^{18}O_c$ field for the Atlantic to available data is found to be instructive. It allows a better understanding of the relative roles of the different parameters within the model. The idea that the $\delta^{18}O_c$ variations in the deep ocean are due, to first order, to temperature changes seems to be quite robust in the model (after subtracting 1.05‰ to account for ice-volume changes). Our analysis points to an underestimation of the changes in simulated deep temperature in CLIMBER-2, an analysis supported by recent data.

Acknowledgements

We wish to thank J.-C. Duplessy for helpful discussions which greatly improved the manuscript and E. Michel for providing benthic foraminiferal $\delta^{18}O_c$ data. We are also grateful to G. Schmidt and A. Mix for constructive reviews and comments during the earlier stage of this work. We are also grateful to G. Delaygue for reviewing the manuscript. This is LSCE contribution 1034.*[BARD]*

References

[1] J. O'Neil, R. Clayton, T. Mayeda, Oxygen isotope fractionation in divalent metal carbonates, J. Chem. Phys. 51 (1969) 5547–5558.

[2] N. Shackleton, Attainment of isotopic equilibrium between ocean water and the benthonic foraminifera genus *Uvigerina*: isotopic changes in the ocean during the last glacial, in: Les méthodes quantitatives d'étude des variations du climat au cours du pléistocène, CNRS Paris, Gif/Yvette, 1974, pp. 203–210.

[3] D. Schrag, G. Hampt, D. Murray, Pore fluid constraints on the temperature and oxygen isotopic composition of the glacial ocean, Science 272 (1996) 1930–1932.

[4] J. Adkins, K. McIntyre, D. Shrag, The salinity, temperature, and $\delta^{18}O$ of the glacial deep ocean, Science 298 (2002) 1769–1773.

[5] G. Schmidt, Oxygen-18 variations in a global ocean model, Geophys. Res. Lett. 25 (1998) 1,201–1,204.

[6] G. Schmidt, Forward modelling of carbonate proxy data from planktonic foraminifera using oxygen isotope tracers tracers in a global ocean model, Paleoceanography 14 (1999) 482–497.

[7] G. Delaygue, J. Jouzel, J.-C. Dutay, Oxygen 18–salinity relationship simulated by an oceanic general circulation model, Earth Planet. Sci. Lett. 178 (2000) 113–123.

[8] CLIMAP, Seasonal reconstructions of the Earth's surface at the last glacial maximum, Map and Chart Ser. #36, Geological Society of America, 1981.

[9] Modellbetreuungsgruppe, The echam3 atmospheric general circulation model, Technical Report 6, Max-Planck Institut für Meteorologie, Hamburg.

[10] G. Hoffmann, M. Werner, M. Heimann, Water isotope module of the ECHAM atmospheric general circulation model: A study on timescale from days to several years, J. Geophys. Res. 103 (1998) 16,871–16,896.

[11] T. Stocker, D. Wright, L. Mysak, A zonally averaged, coupled ocean-atmosphere model for paleoclimate studies, J. Clim. 5 (1992) 773–797.

[12] V. Petoukhov, A. Ganopolski, V. Brovkin, M. Claussen, A. Eliseev, C. Kubatzki, S. Rahmstorf, CLIMBER-2: a climate system model of intermediate complexity. Part I: model description and performance for present climate, Clim. Dyn. 16 (2000) 1–17.

[13] A. Ganopolski, S. Rahmstorf, V. Petoukhov, M. Claussen, Simulation of modern and glacial climates with a coupled model of intermediate complexity, Nature 391 (1998) 351–356.

[14] M. Kageyama, O. Peyron, S. Pinot, P. Tarasov, J. Guiot, S. Joussaume, G. Ramstein, The Last Glacial Maximum climate over Europe and western Siberia: a PMIP comparison between models and data, Clim. Dyn. 17 (2001) 23–43.

[15] A. Ganopolski, S. Rahmstorf, Rapid changes of glacial climate simulated in a coupled climate model, Nature 409 (2001) 153–158.
[16] G. Schmidt, G. Bigg, E. Rohling, Global seawater oxygen-18 database, http://www.giss.nasa.gov/data/o18data/.
[17] G. Bigg, E. Rohling, An oxygen isotope data set for marine water, J. Geophys. Res. 105 (2000) 8527–8535.
[18] G. Farquhar, J. Llyod, J. Taylor, L. Flanagan, J. Syvertsen, K. Hubick, S. Wong, Vegetation effects on the isotope composition of oxygen in atmospheric CO_2, Nature 363 (1993) 439–443.
[19] L. Merlivat, J. Jouzel, Global climatic interpretation of the deuterium-oxygen 18 relationship for precipitation, J. Geophys. Res. 84 (1979) 5029–5033.
[20] M. Majoube, Fractionnement en oxygène 18 entre l'eau et sa vapeur, J. Chim. Phys. 68 (1971) 1423–1436.
[21] M. Wadley, G. Bigg, E. Rohling, A. Payne, On modelling present-day and last glacial maximum oceanic $\delta^{18}O$ distributions, Global Planet. Change 32 (2002) 89–109.
[22] R.W. Peltier, Ice-age paleotopography, Science 265 (1994) 195–201.
[23] J. Duplessy, L. Labeyrie, C. Waelbroeck, Constraints on the oxygen isotopic enrichment between the Last Glacial Maximum and the Holocene: Paleoceanographic implications, Quat. Sci. Rev. 21 (2002) 315–330.
[24] J.-C. Duplessy, L. Labeyrie, A. Juillet-Leclerc, F. Maitre, J. Duprat, M. Sarnthein, Surface salinity reconstruction of the North Atlantic Ocean during the last glacial maximum, Oceanol. Acta 14 (1991) 311–324.
[25] J. Lynch-Stieglitz, R. Fairbanks, Glacial-interglacial history of antarctic intermediate water/relative strengths of Antarctic versus Indian ocean sources, Paleoceanography 9 (1994) 7–29.
[26] E. Michel, L. Labeyrie, J.-C. Duplessy, N. Gorfti, M. Labracherie, J. Turon, Could deep subantarctic convection feed the world deep basins during the last glacial maximum?, Paleoceanography 10 (1995) 927–942.
[27] U. Ninnemann, C. Charles, Regional differences in Quaternary subantarctic nutrient cycling link to intermediate and deep water ventilation, Paleoceanography 12 (1997) 560–567.
[28] D. Oppo, M. Horowitz, Glacial deep water geometry: South Atlantic benthic foraminiferal Cd/Ca and $\delta^{13}C$ evidence, Paleoceanography 15 (2000) 147–160.
[29] N. Slowey, W. Curry, Glacial-interglacial differences in circulation and carbon cycling within the upper western North Atlantic, Paleoceanography 10 (1995) 715–732.
[30] T. Marchitto, W. Curry, D. Oppo, Millennial-scale changes in North Atlantic circulation since the last glaciation, Nature 393 (1998) 557–561.
[31] D. McCorkle, D. Heggie, H. Veeh, Glacial and Holocene stable isotope distributions in the southeastern Indian Ocean, Paleoceanography 13 (1998) 20–34.
[32] M. Huels, Millennial-scale SST variability as inferred from planktonic foraminifera census counts in the western subtropical Atlantic, Technical Report, GEOMAR, Kiel, 2000.
[33] J. Duplessy, N. Shackleton, R. Fairbanks, L. Labeyrie, D. Oppo, N. Kallel, Deep water source variations during the last climatic cycle and their impact on the global deepwater circulation, Paleoceanography 3 (1988) 343–360.
[34] M. Sarnthein, K. Winn, S. Jung, J.-C. Duplessy, L. Labeyrie, H. Erlenkeuser, G. Ganssen, Change in the east Atlantic deepwater circulation over the last 30,000 years: Eight time slice reconstructions, Paleoceanography 9 (1994) 209–267.
[35] T. Machitto, D. Oppo, W. Curry, Paired benthic foraminiferal Cd/Ca and Zn/Ca evidence for a greatly increased presence of Southern Ocean Water in the glacial North Atlantic, Paleoceanography 17 (2002) 10.1–10.16.